*Applied Chemical Engineering (2026) Volume 9 Issue 1* ISSN: 2578-2010 (O)
doi: 10.59429/ace.v9i1.5884

ORIGINAL RESEARCH ARTICLE

# A novel method for the remediation of environmental impacts of oil spills using poly carboxymethylcellulose coated ($Fe_2O_3$, $Al_2O_3$, and Ag) nanoparticles

**Khamael Abd Alsalam [1*], Mohamed Ali Mutar [2]**

[1] *Department of Environment, College of Science, University of AL-Qadisiyah, Iraq*

[2] *Department of Chemistry, College of Science, University of AL-Qadisiyah, Iraq*

***Corresponding author:** Khamael Abd Alsalam; Khamael abdulsalam@qu.edu.iq

## ABSTRACT

Large-scale oil spills and the discharge of oily effluents from ships and industrial operations pose serious environmental threats and often result in significant economic consequences. Conventional cleanup methods remain largely ineffective and may themselves cause ecological damage, yet nanotechnology offers a promising alternative for addressing oil contamination. In this study, polycarboxymethycellulose-coated nanoparticles (Fe2O3, Al2O3, and Ag) were synthesized via a simple, cost-effective hydrothermal technique and applied to remove Basra crude oil (API-32) from synthetic seawater under realistic environmental conditions. The physicochemical properties of these materials were characterized using FTIR and SEM analyses, while fluorescence and proton nuclear magnetic resonance spectroscopy confirmed near-complete oil-water separation under optimized conditions. Gas chromatography-mass spectrometry results showed that approximately 100 percent of lower molecular weight alkanes (C9–C21) were eliminated within 6 hours, and extending treatment to 24 hours removed more than 67 percent of C22–C25 alkanes. Among the tested materials, CMC-coated Ag nanoparticles demonstrated the highest removal efficiency at an optimal loading of 1.6 wt percent, with disintegration order following Ag > Fe2O3 > Al2O3. The superior performance of nano-Ag is attributed to its greater surface area, smaller particle size, homogeneous morphology, and strong oil adsorption capacity. Additionally, preliminary investigations assessed potential genotoxic effects and, for the first time, examined the ability of these nanoparticles to mitigate crude oil-induced genotoxicity in vivo, confirming their potential for rapid and effective oil removal.

***Keywords:*** Remediation;Oil Spills; Carboxymethylcellulose; Nanoparticles; Polymer Coated.

**ARTICLE INFO**

Received: 13 January 2026
Accepted: 5 February 2026
Available online: 12 February 2026



## Graphical Abstract

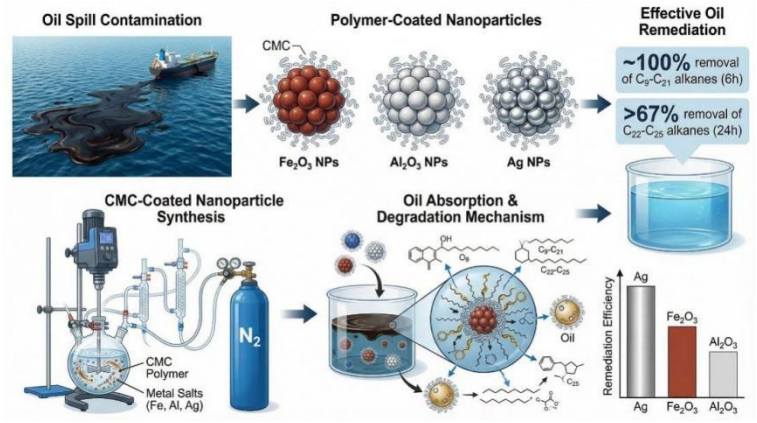

# 1. Introduction

The release of petroleum and oil-based pollutants through industrial waste, shipping activities, and accidental spills causes severe harm to marine and aquatic environments. The Deepwater Horizon disaster in 2010 serves as a stark reminder, when more than 4.9 million barrels of crude oil entered the Gulf of Mexico and devastated vital ecosystems. Ships contribute significantly to this problem by producing large quantities of bilge water, which contains water mixed with lubricants and various contaminants. [2] Pipelines also constitute a primary source of inland water pollution, and spills in these areas often present greater public health risks than coastal incidents due to their proximity to freshwater supplies and densely populated regions. Such oily wastes damage both coastal and freshwater ecosystems while causing substantial economic losses. [4] Oil contamination disrupts animal feeding patterns, degrades habitats, produces ecotoxicological effects on wildlife, and threatens the health of communities dependent on these natural resources. [5, 6] Current oil spill response techniques include skimming devices, in situ burning, chemical dispersants, and sorbents, though each method demonstrates limited effectiveness depending on spill conditions. Booms, for instance, struggle to contain oil effectively, require costly maintenance, and cannot prevent oil from sinking. Skimming systems work best with thick oil layers and calm waters but collect considerable amounts of water requiring subsequent treatment. [7] In situ burning necessitates boom deployment to concentrate oil, and its success depends heavily on weather conditions. Dispersants temporarily increase oil dispersion into the water column but offer only short-term benefits, restricting their application near sensitive benthic ecosystems like coral reefs. [8] Although most petroleum hydrocarbons undergo biodegradation in aerobic conditions, this process slows considerably in anaerobic environments or when oil concentrations are high, limiting bioremediation potential. [9] Oil-water separators used aboard ships require substantial space and expensive post-treatment to meet discharge standards. Given these limitations, researchers continue seeking alternative approaches, with nanotechnology emerging as a particularly promising field. [10, 11] Nanotechnology involves utilizing nanoparticles ranging from 1 to 100 nm and has attracted considerable scientific attention. [12] Iron oxide nanoparticles offer notable advantages owing to their low toxicity and magnetic properties, enabling easy separation from liquids. [13-15] Studies have demonstrated that magnetite nanoparticles combined with superhydrophobic polyester materials achieve highly selective oil absorption. Thermal decomposition-derived magnetic composites have proven effective for oil-water separation, with efficiency varying based on coating materials. [16] Superhydrophobic magnetic bulk materials also exhibit strong oil absorption capabilities. [18, 19] However, many synthesis methods require multiple steps, organic solvents, and elevated temperatures, creating challenges for industrial-scale production. Nanoremediation leverages the superior surface-area-to-volume ratio of nanomaterials compared to their macroscale counterparts, enabling enhanced pollutant modification or degradation. [20] This paper examines current remediation practices, the growing adoption of nanoremediation, and opportunities for further research and technological advancement.

# 2. Experimental

## 2.1. Materials

The materials utilized in this study were as follows: carboxymethylcellulose (CMC, purity ≥99.5%, HiMedia Laboratories Pvt. Ltd., India), $Fe_2O_3$ nanoparticles (purity ≥99%, British Drug Houses [BDH], UK), $Al_2O_3$ nanoparticles (purity ≥99%, BDH, UK), silver nanoparticles (purity ≥99.9%, Merck KGaA, Germany), Basra crude oil (API-32, obtained from the Basra Oil Company, Iraq), and synthetic seawater (prepared in the laboratory according to standard protocols).

## 2.2. Crude oil

The experimental study has been performed on a Basra crude oil sample. Crude oil's physical characteristics have been listed in **Table 1** and then analyzed in Daura refinery.

**Table 1.** Physical Characteristics of Basra Crude Oil (Daura refinery).

| Properties | Basra Crude Oil |
|---|---|
| SpGr. at 15.6°C | **0.88490** |
| Salt contents (%wt.) | **0.00060** |
| API | **28.40** |
| Asphaltenes (%wt.) | **2.220** |
| Sediment and Water content (%vol.) | **0.050** |
| Sulfur contents (%wt.) | **2.10** |
| Viscosity (cp) at $20^{0}$C | **50** |
| Ash contents (%wt.) | **0.01510** |
| Conductivity (mS) | **0** |

## 2.3. The laboratory system for studying the removal of oil slicks

A glass-based laboratory apparatus was designed and constructed to simulate water contamination conditions associated with oil slicks. The primary objective of this experimental setup was to investigate the physicochemical properties of the synthesized polymer-coated nanoparticles and evaluate their effectiveness in dispersing oil slicks. The system comprised a locally fabricated glass basin with dimensions of 50 cm (length) × 40 cm (width) × 30 cm (height). For each experimental trial, 5 mL of crude oil was introduced into the system. This particular oil volume was selected based on previously reported literature values and the assumption that spilled oil distributes uniformly within the upper 5 cm layer of the water column following a spill event.

**Figure 1.** The laboratory system for removing oil slicks. Basin dimensions: 50 cm (length) × 40 cm (width) × 30 cm (height).[3].

## 2.4. Instruments

Several analytical techniques were employed to characterize the prepared nanoparticles and evaluate their oil removal performance. Fourier transform infrared (FTIR) spectroscopy was performed using a TENSOR 27 spectrometer (BRUKER, Germany) at the College of Engineering, University of Al-Qadisiyah. The morphological characteristics and distribution of nanoparticles were examined by scanning electron microscopy (SEM) using a FEI Nova Nano SEM 230 instrument (Eindhoven, Netherlands), located at the Electron Microscopy Unit in Iran. Fluorescence measurements were conducted using a Spectrofluorometer (Shimadzu, Model RF-5301 PC) at the College of Science, University of Al-Qadisiyah. Gas chromatography-

mass spectrometry (GC-MS) analysis was carried out using a Shimadzu spectrometer (Model: NIS11 LIBRAR JE) to identify and quantify the petroleum hydrocarbon components before and after treatment.

### 2.5. Synthesis of polymer-coated nanoparticles (Fe2O3, AL2O3, Ag)

Under ambient air conditions, polymer-coated nanoparticles (NPs) were created using a quick and inexpensive hydrothermal synthesis technique. The synthesis techniques have been previously published with changes. The polymer-coated nanoparticles were made by mixing 25 mL of ultrahigh quality water and 3.6 g of polymer (carboxymethylcellulose) at 80 °C for 10 minutes. The solution was swirled at 80°C. $Fe_2O_3$, $AL_2O_3$, and Ag nanoparticles (0.2, 0.4, 0.6, 0.8, 1, 1.2, 1.4, 1.6, and 1.8) were added to the solution and agitated for another 10 minutes at 80 °C. Sonication was used to re-distribute the suspension in water. For the experiment on oil removal, NPs solutions were kept.

**Figure 2.** Polymer-coated nanoparticles (Nanosolution) experiment

## 3. Results and discussions

### 3.1. Characterization

#### 3.1.1. FTIR Spectrum of CMC- Fe2O3

FTIR spectroscopic analysis was employed to characterize the structural features of CMC-$Fe_2O_3$, CMC-$Al_2O_3$, and CMC-Ag nanocomposites, as illustrated in **Figures 3, 4, and 5**, respectively. The recorded spectra of CMC-$Fe_2O_3$ samples exhibited characteristic absorption bands at 577 $cm^{-1}$ and 477 $cm^{-1}$, which are attributed to Fe-O stretching vibrations typical of $Fe_2O_3$. Absorption peaks corresponding to adsorbed water ν(OH) appeared at 3554 $cm^{-1}$ and 3324 $cm^{-1}$, while the characteristic vibrations of $CH_2$ and O-CH groups were detected at 1675 $cm^{-1}$, 1433 $cm^{-1}$, and 1383 $cm^{-1}$. A prominent broad band observed at 3434 $cm^{-1}$ can be ascribed to hydroxyl groups as well as intermolecular and intramolecular hydrogen bonding interactions within the polymer matrix. The intense band at 1595 $cm^{-1}$ is indicative of asymmetric stretching vibrations of carboxylate groups ($COO^-$), whereas bands appearing at 1186 $cm^{-1}$ and 968 $cm^{-1}$ arise from CH-O-$CH_2$ stretching modes [22-24]. Similarly, the FTIR spectrum of CMC-$Al_2O_3$ nanocomposite displayed absorption features consistent with the CMC backbone, with bands at essentially the same wavenumbers for ν(OH), $CH_2$, and O-CH vibrations. The spectral profile confirmed the successful incorporation of aluminum oxide into the carboxymethyl cellulose structure while maintaining the fundamental polymer characteristics [22-24]. In the case of CMC-Ag nanocomposite, FTIR analysis revealed that while the characteristic CMC absorption bands remained largely unchanged, the spectrum exhibited a distinct peak at 476 $cm^{-1}$ which is associated with the presence of $Ag^+$ ions in the CMC-AgNPs composite. The vibrations attributed to adsorbed water, hydroxyl, methylene, and ether linkages were observed at their expected positions, along with the broad hydrogen bonding band at 3434 $cm^{-1}$. The carboxylate stretching at 1595 $cm^{-1}$ and the CH-O-$CH_2$ stretching bands at 1186 $cm^{-1}$ and 968 $cm^{-1}$ further confirmed the preservation of the CMC structure following silver nanoparticle incorporation [22-24].

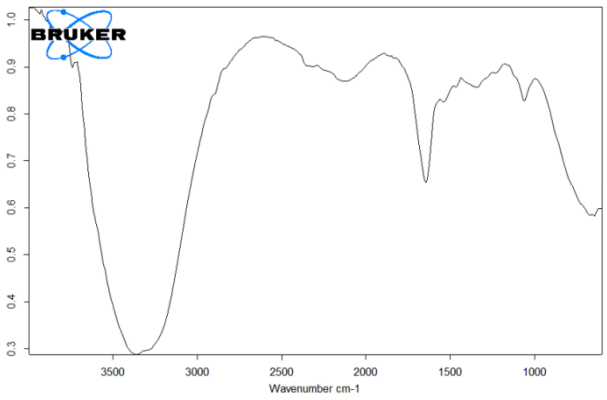


**Figure 3.** FTIR Spectrum of CMC-$Fe_2O_3$

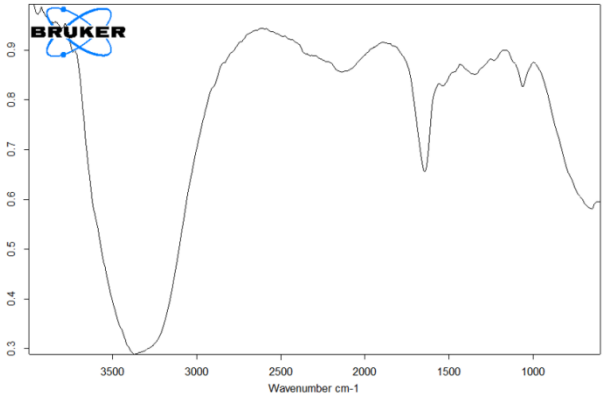


**Figure 4.** FTIR Spectrum of CMC-$Al_2O_3$

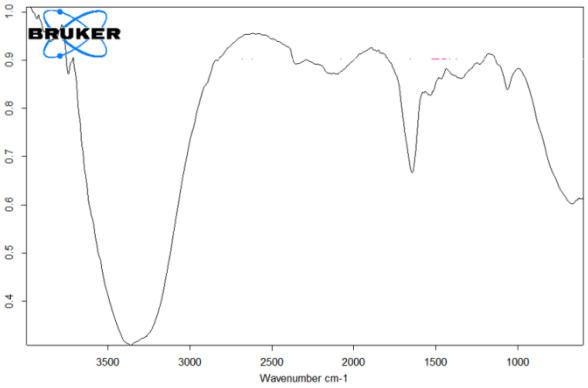


**Figure 5.** FTIR Spectrum of CMC-Ag

## 3.2. Scanning Electron Microscopy (SEM)

### 3.2.1. SEM of Carboxymethylcellulose-coated Fe2O3 nanoparticles

Scanning electron microscopy (SEM) was employed to investigate the surface morphology and topographical features of the synthesized nanomaterials. The SEM micrographs of CMC-coated $Fe_2O_3$ nanoparticles are presented in **Figures 6, 7, and 8**. The individual particles exhibited a nearly spherical morphology, though the extent of agglomeration varied considerably depending on the support material. In the case of $Fe_2O_3$ nanoparticles, a reasonably uniform distribution with minimal aggregation was observed. However, when incorporated into the CMC matrix, significant particle agglomeration occurred, resulting in incomplete surface coverage by $Fe_2O_3$, which may consequently affect the photocatalytic performance. The SEM images captured at magnifications of 5 µm and 2 µm clearly reveal the size distribution, morphological

characteristics, and layered architecture of the nanosolution (**Figure 6**). Furthermore, **Figure 7** illustrates the SEM analysis of carboxymethylcellulose loaded with varying weight percentages of $Fe_2O_3$ ranging from 0.2 to 1.6 wt%. At higher magnifications of 500 nm and 200 nm (**Figure 8**), successful dispersion of nanoparticles across the carboxymethylcellulose surface becomes evident, exhibiting homogeneous distribution and remarkable stability. The relatively small particle dimensions facilitated uniform spreading on the polymer substrate. The SEM characterization of CMC-coated $Al_2O_3$ nanoparticles is depicted in **Figures 9 and 10**. The micrographs clearly demonstrate that the $Al_2O_3$ surface possesses a rough texture with quasi-spherical particle geometry, having an average diameter in the range of 200-500 nm [25]. These nanoparticles display distinct crystalline features that render them suitable for coating applications. Following the coating process, the $Al_2O_3$ nanoparticles exhibited increased thickness, with the average diameter expanding to approximately 1 µm, confirming successful attachment of the coating material to the nanoparticle surface. The dispersion of $Al_2O_3$ nanoparticles on the carboxymethylcellulose surface proved highly effective, attributed primarily to the elevated nanoparticle concentration. Images obtained at 5 µm and 2 µm magnifications (**Figure 10**) provide detailed visualization of the particle dimensions, morphology, and the multilayered structure of the nanosolution. The morphological characteristics of CMC-coated Ag nanoparticles were examined using SEM, as shown in **Figures 11 and 12**. The SEM images captured silver nanoparticles synthesized via CMC on drop-coated substrates, providing valuable insights into their size, shape, and overall morphology. The analysis revealed that the AgNPs exhibited spherical, polydisperse morphologies with particle sizes ranging from 200 to 500 nm. It is worth noting that manipulation of the synthesis environment enables control over both the size and shape of the resulting silver nanoparticles. The surface appeared smooth throughout, with a well-defined network structure. Additional SEM images acquired at magnifications of 5 µm and 2 µm (**Figure 12**) further elucidate the structural organization and multiple layers present within the nanosolution.

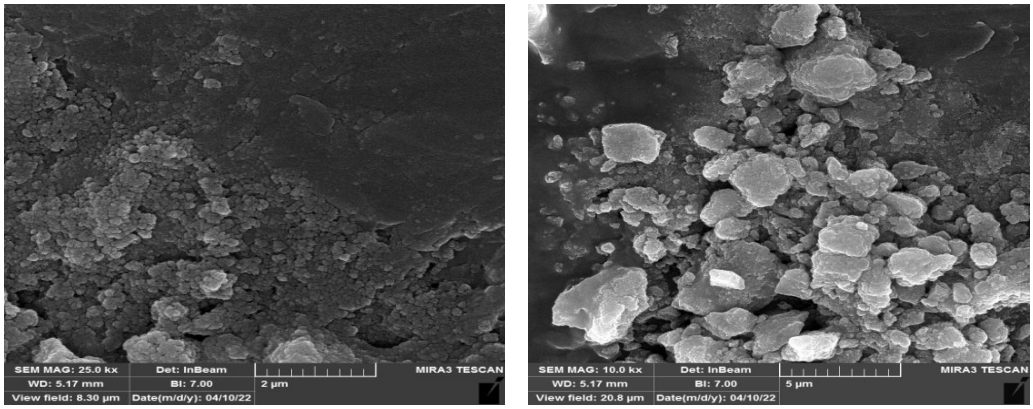


**Figure 6.** SEM image of CMC-coated $Fe_2O_3$ nanoparticles at magnifications of 5 µm and 2 µm.

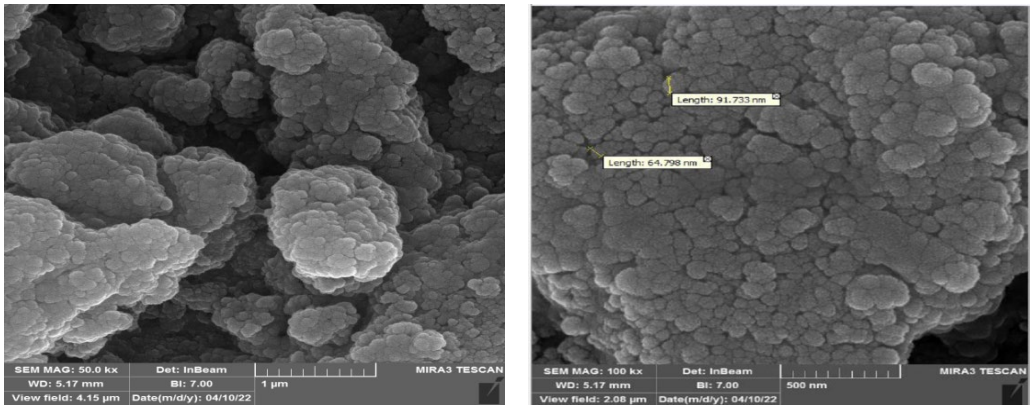

**Figure 7.** SEM image of $Fe_2O_3$ nanoparticles coated with CMC.

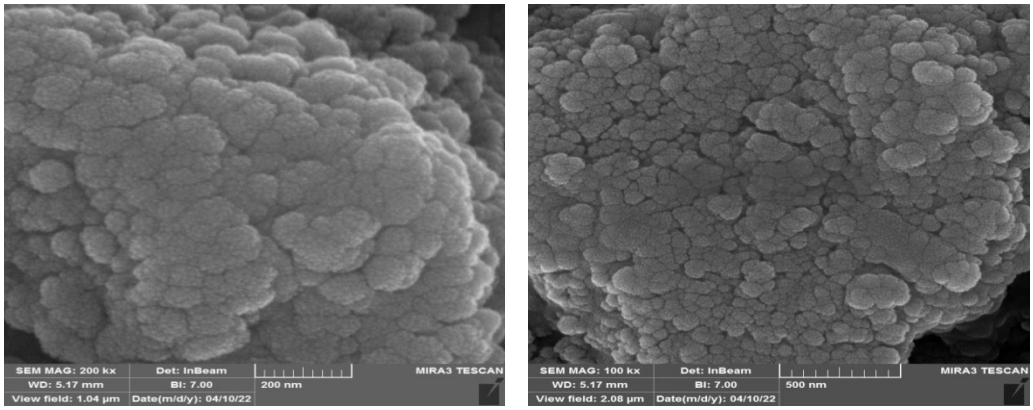


**Figure 8.** SEM image of CMC-coated $Fe_2O_3$ nanoparticles at magnifications of 500 nm and 200 nm.

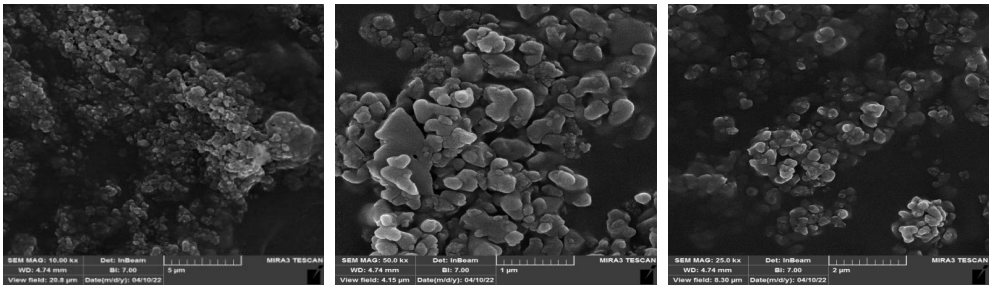

**Figure 9.** SEM image of CMC-coated $Al_2O_3$ nanoparticles with diameter between 200-500 nm and 1 µm.

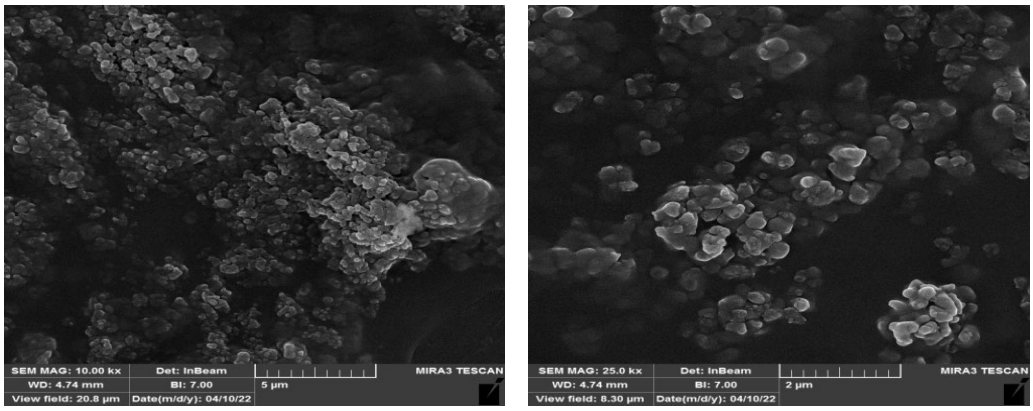


**Figure 10.** SEM image of CMC-coated $Al_2O_3$ nanoparticles at magnifications of 5 µm and 2 µm.

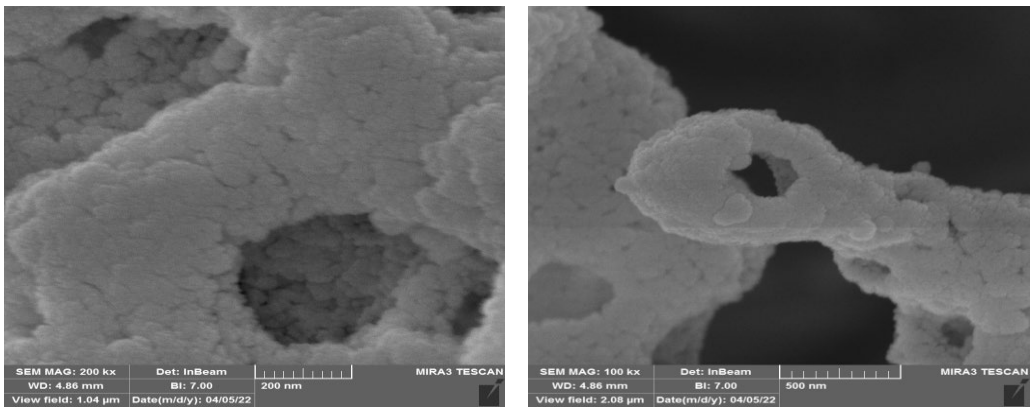

**Figure 11.** SEM image of CMC-coated Ag nanoparticles at magnifications of 200 nm and 500 nm.

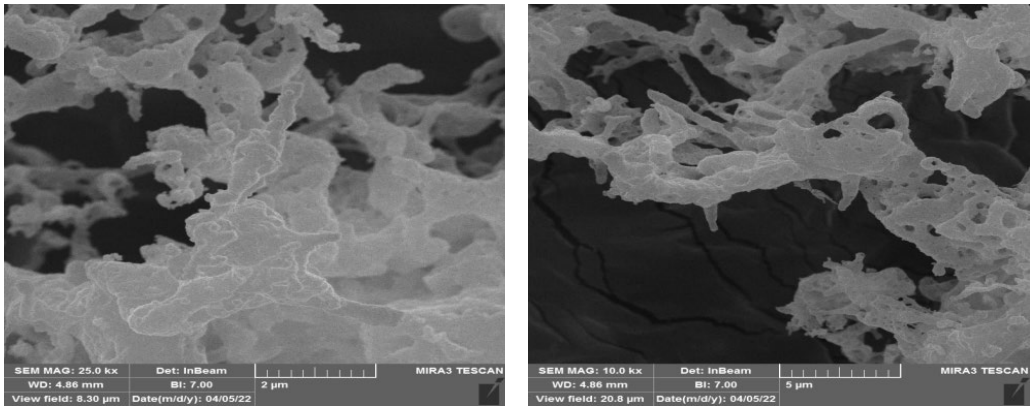


**Figure 12.** SEM image of CMC-coated Ag nanoparticles at magnifications of 5 µm and 2 µm.

### 3.2.2. Oil Removal from High Purity Water using CMC-coated Nanoparticles (Fe2O3, Al2O3, and Ag)

Various NP concentrations (0.2-1.8 wt%) were tested to optimize oil removal efficiency. The fluorescence spectra for oil experiments in ultrapure water after 6 and 24 hours separation are presented in **Figures 13-16**. Results showed that oil removal increased from 65.2% to nearly 100% as NP concentration rose from 0.2 to 1.8 wt%, with decreased fluorescence intensity indicating enhanced aromatic hydrocarbon elimination. However, at 1.8 wt% NP concentration, removal slightly decreased to 88.7% due to NP aggregation reducing surface area and adsorption capacity.

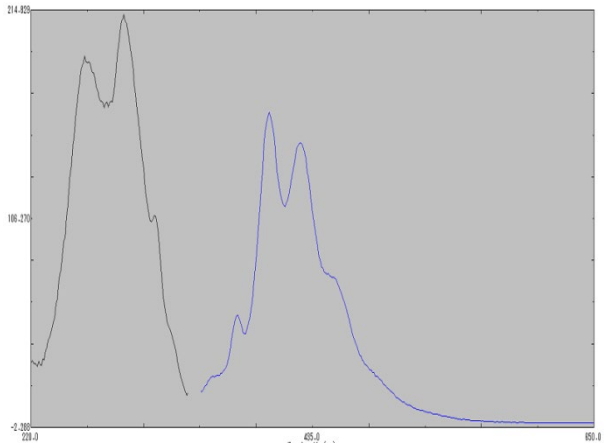

**Figure 13.** Fluorescence spectra of the WAF sample before NPs addition.

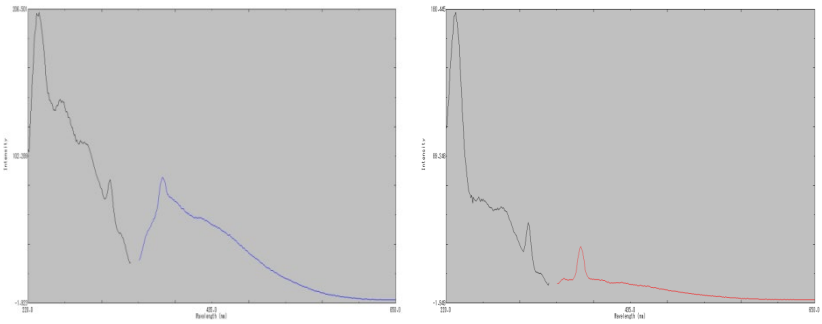

(a) 6 hour (b) 24 hour

**Figure 14.** Fluorescence spectra after NPs addition (1.6% $Fe_2O_3$) for 6 & 24 hours.

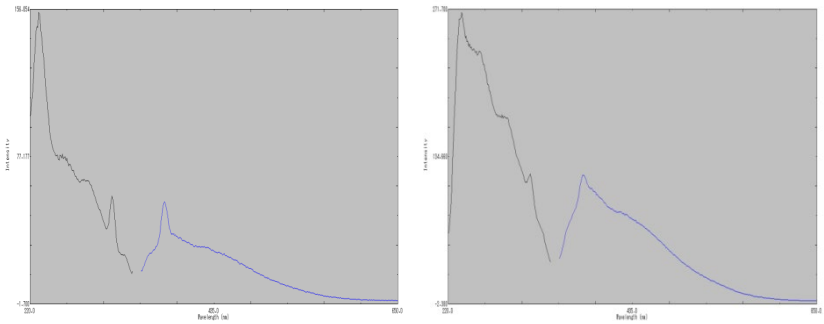

(A) 6 hour (B) 24 hour

**Figure 15.** Oil removal after 6 and 24 hours.

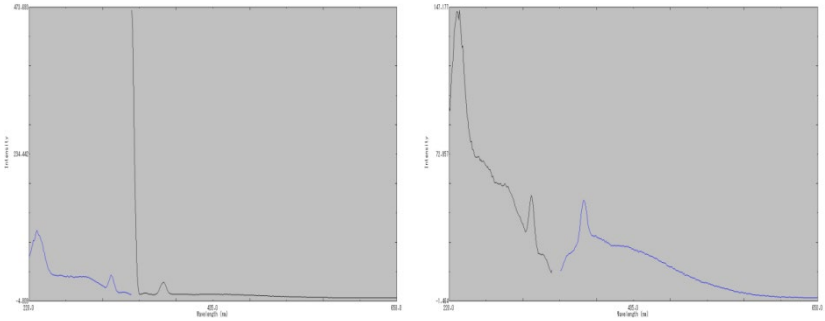

(a) 6 hour (b) 24 hour

**Figure 16.** Oil removal after 6 and 24 hours of use.

To examine separation time effects, individual tests were conducted using optimal NP concentration (1.2%). Fluorescence data showed oil removal increased from 68% to 100% when separation time extended from 6 to 24 hours (**Figure 17**). The water-soluble fraction of crude oil, rich in aromatic hydrocarbons, is highly toxic to marine organisms, particularly in early life stages [25]. This study utilizes $Fe_2O_3$, $Al_2O_3$, and Ag nanoparticles to reduce oil pollution in seawater, which would benefit marine life protection and aquaculture.

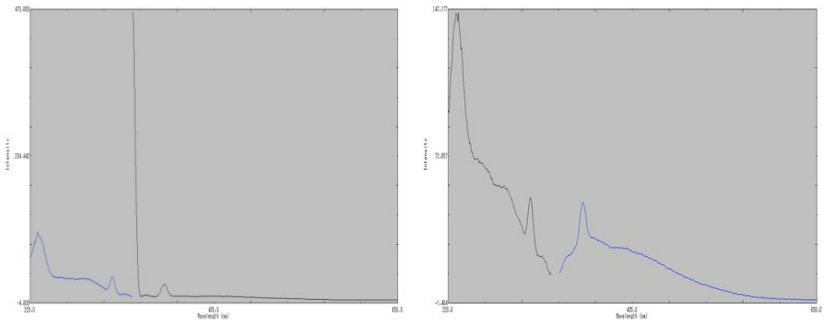

(a) 6 hour (b) 24 hour

**Figure 17.** Fluorescence spectra after optimized NP concentration (1.2%) for 6 and 24 hours.

GC-MS analysis revealed that chromatogram peaks of residual oil samples were significantly reduced compared to original oil-water mixture, demonstrating excellent alkane removal by CMC-coated NPs. After six hours, all lower chain alkanes (C9-C21) were completely eliminated, while longer chain alkanes (C22-C25) showed >67% removal. The identified hydrocarbons comprise 73% of total saturated hydrocarbons [26]. **Figures 18-21** illustrate the GC-MS results for PAH and TPH removal/degradation.

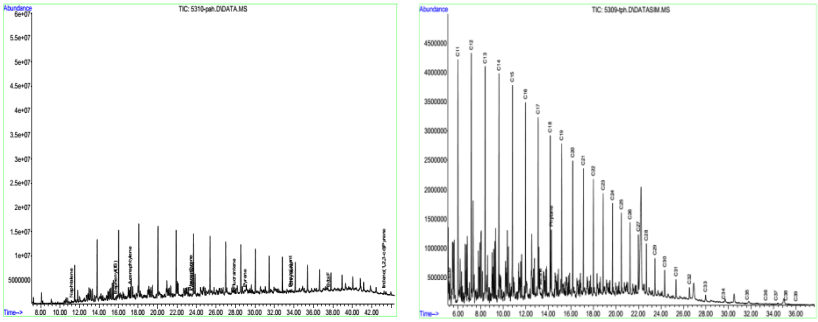

PAH TPH

**Figure 18.** GC-MS analysis of crude oil prior to NPs addition.

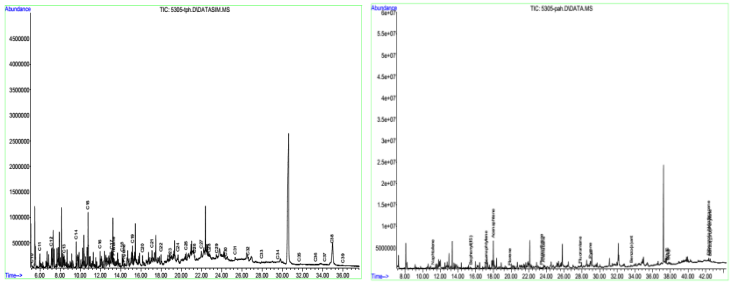

(a) PAH - 6 hour TPH - 6 hour

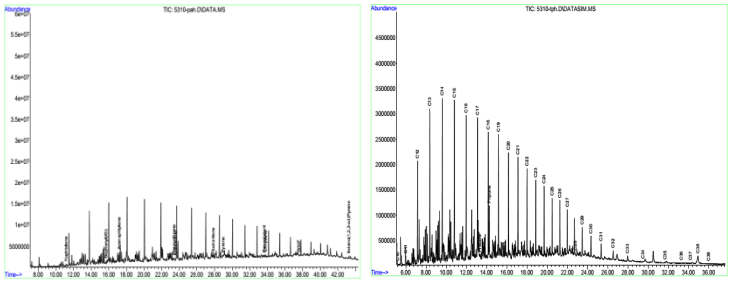

(b) PAH - 24 hour TPH - 24 hour

**Figure 19.** GC-MS results by CMC-coated $Fe_2O_3$ NPs after 6 and 24 hours.

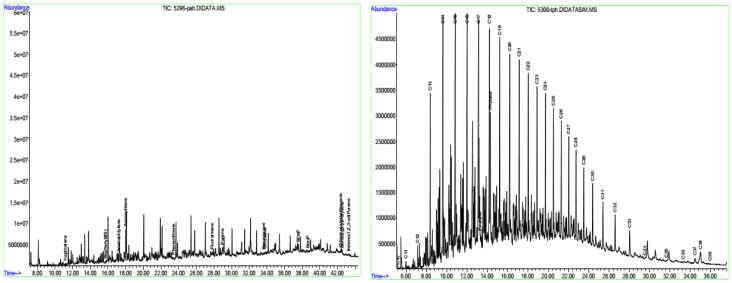

(A) PAH - 6 hour TPH - 6 hour

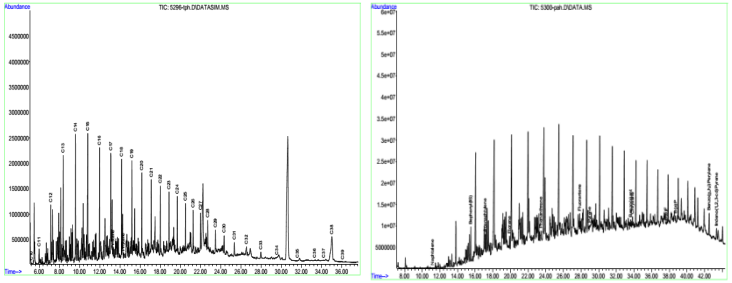

(B) PAH - 24 hour TPH - 24 hour

**Figure 20.** GC-MS results by CMC-coated $Al_2O_3$ NPs for 6 & 24 hours.

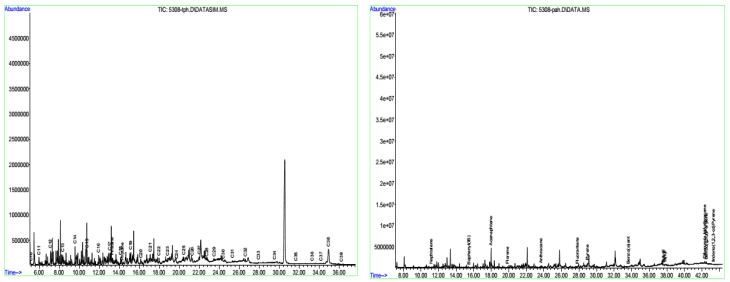

(A) PAH - 6 hour TPH - 6 hour

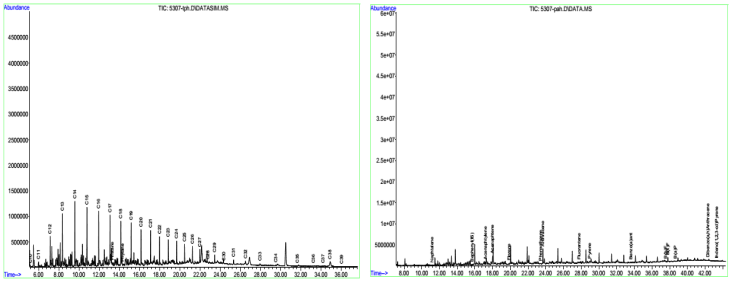

(B) PAH - 24 hour TPH - 24 hour

**Figure 21.** GC-MS results by CMC-coated Ag NPs for 6 & 24 hours.

The optimal nanoparticle loadings were determined as 1.6 wt% for $Fe_2O_3$, 1.6 wt% for $Al_2O_3$, and 1.2 wt% for Ag. Excessive catalyst loading causes agglomeration, reducing photocatalytic efficiency. Oil sorption is driven by hydrophobic interactions between CMC fractions and hydrocarbons [27]. Higher ionic strength improves separation through enhanced agglomeration from reduced electrostatic repulsion and improved bridging flocculation [28], with magnetic separation being more efficient on aggregated NPs [29].

These NPs demonstrate outstanding removal efficiency in laboratory conditions. Conventional methods recover only ~16% of spilled oil [30]. Assuming each NP sorbs 30 times its mass of oil, approximately $3.5 \times 10^6$ kg NPs would remove equivalent oil quantities [29]. Since NPs can be reused, actual requirements may be lower. The main barrier to large-scale adoption is rapid synthesis capacity, though the approach is immediately applicable for smaller-scale oil emissions with proper environmental deployment strategies [30].

### 3.2.3. Effect of CMC-coated Nanoparticles (Fe2O3, Al2O3, and Ag) on Oil Removal in Seawater

This section details the investigation into the effectiveness of nano-solutions composed of polymer-coated nanoparticles for dissolving oil slicks [5]. To simulate oil-contaminated water, 5 ml of Basra crude oil was placed in a glass basin containing approximately 5 liters of water. Various amounts of $Fe_2O_3$, $Al_2O_3$, and Ag nanoparticles were added, and oil slick disintegration rates were measured over time intervals of 1, 2, 3, 4, 5, 6, and 24 hours. The proportion of crude oil released during treatment was calculated spectrophotometrically. **Figure 22** depicts the oil spot floating on the water surface before nano-solution application [3].

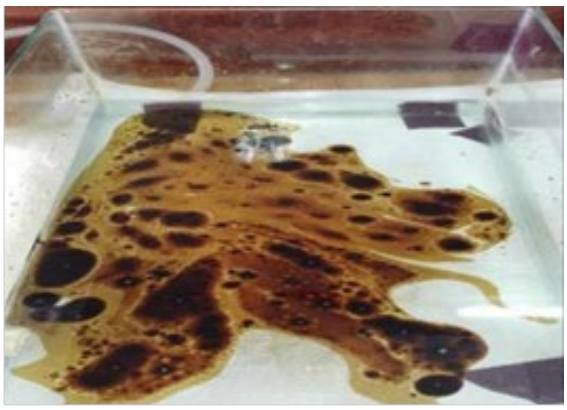

**Figure 22.** The contaminated oil slick on the basin water surface.

The experiments utilized nano-solutions containing varied concentrations of $Fe_2O_3$, $Al_2O_3$, and Ag nanoparticles treated with CMC at weight percentages of 0.2, 0.6, 0.8, 1.0, 1.2, 1.4, 1.6, and 1.8. Oil removal percentages were calculated at 6 and 24 hours for each concentration, as shown in **Figures 23, 24, and 25**.

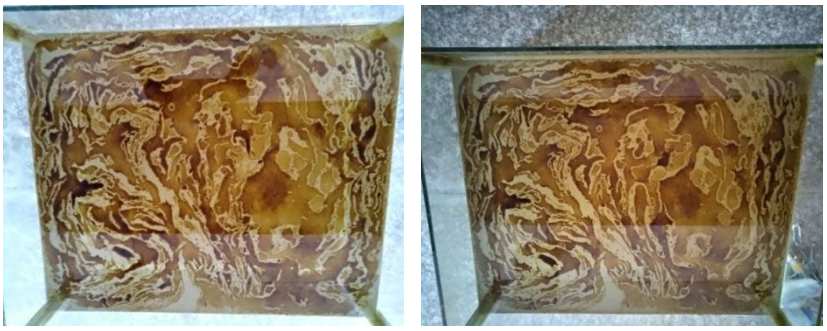

**Figure 23.** Oil slick disintegration after 6 and 24 hours of CMC-coated $Fe_2O_3$ NPs.

**Figure 24.** Oil slick disintegration after 6 and 24 hours of CMC-coated $Al_2O_3$ NPs.

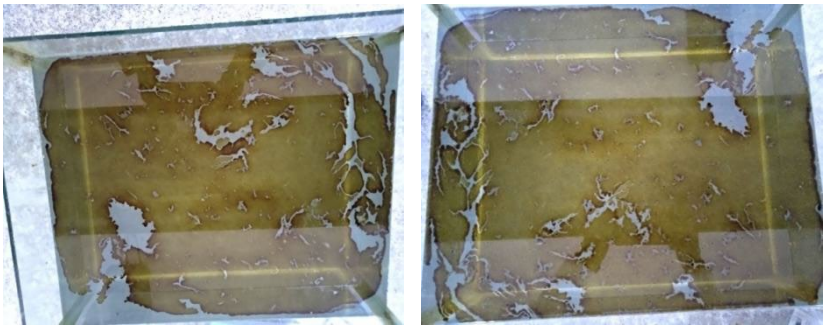

**Figure 25.** Oil slick disintegration after 6 and 24 hours of CMC-coated Ag NPs.

For CMC-coated $Fe_2O_3$ nanoparticles, the disintegration rate was particularly significant during the first six hours due to the large surface area and widespread distribution of the nanomaterial over the polymeric surface. After 24 hours, 98% of oil slicks had disintegrated (**Figures 26-28**). The rapid initial disintegration is attributed to the greater surface area available for absorption at the beginning. The optimal concentration was found to be 1.6 wt%, achieving 97% oil removal [30].

**Figure 26.** Oil slick disintegration after 1 and 24 hours of CMC-coated $Fe_2O_3$ NPs.

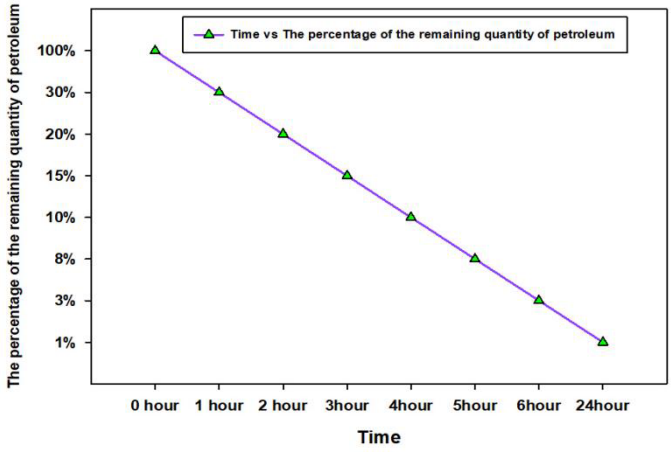


**Figure 27.** Percentage of remaining petroleum with CMC-$Fe_2O_3$ solution (1.6%) over time.

**Figure 28.** Oil slick disintegration after 24 hours of CMC-coated $Fe_2O_3$ NPs.

Similar results were observed for CMC-coated $Al_2O_3$ nanoparticles (**Figures 29-30**). The absorption rate was high during the first six hours due to the large surface area and wide distribution of $Al_2O_3$ nanoparticles

over the CMC surface. After 24 hours, 98% of oil traces were removed at the optimal concentration of 1.6 wt%.

**Figure 29.** Oil slick disintegration after 1 and 6 hours of CMC-coated $Al_2O_3$ NPs.

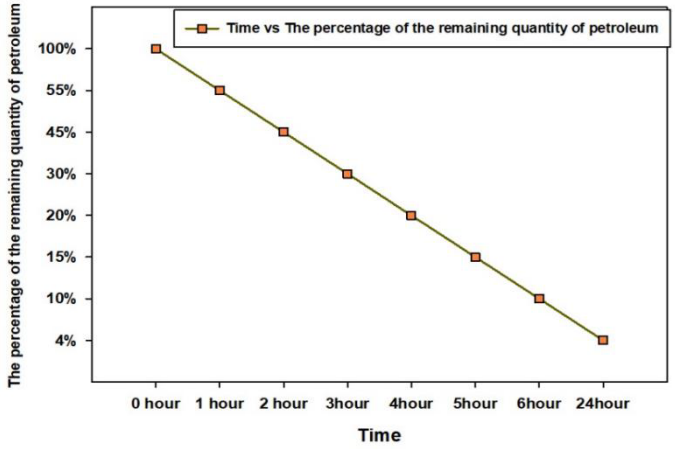


**Figure 30.** Percentage of remaining petroleum with CMC-$Al_2O_3$ solution (1.6%) over time.

When 1.2 wt% of CMC-coated Ag nanoparticles were used, oil stain removal reached 100%, surpassing both $Al_2O_3$ and $Fe_2O_3$ (**Figures 31-32**). The superior performance of Ag nanoparticles is attributed to their increased surface area due to smaller particle sizes, higher surface energy at filler-matrix interfaces, homogeneous morphology, and strong oil adsorption capability [12,26]. The disintegration order was: Ag > $Fe_2O_3$ > $Al_2O_3$.

**Figure 31.** Oil slick disintegration after 1 and 6 hours of CMC-coated Ag NPs.

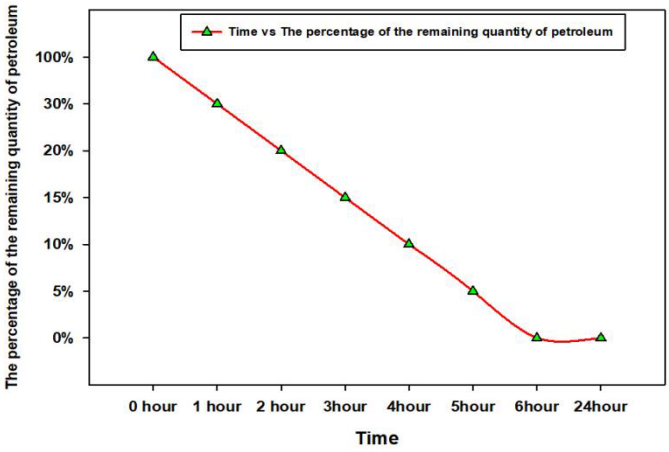


**Figure 32.** Percentage of remaining petroleum with CMC-Ag solution (1.2%) over time.

### 3.2.4. Toxicity

In this pilot investigation, pure polymer-coated (CMC, MC, PEG) nanoparticles ($Fe_2O_3$, $Al_2O_3$, and Ag) were examined for their potential to inhibit WAF crude oil genotoxicity in vivo for the first time. The water-accommodated fraction (WAF) represents maximum concentrations of dissolved petroleum hydrocarbons in spills, comprising phenols, heterocyclic compounds, and mono-aromatic chemicals including benzene, toluene, ethyl benzene, and xylene [5,9]. WAF contains the most hazardous chemicals for aquatic species [25].

### 3.2.5. Antibacterial Activity of Polymer-coated Nanoparticles

Biogenic $Fe_2O_3$, $Al_2O_3$, and Ag NPs coated with CMC, MC, and PEG were tested against B. subtilis using agar well diffusion technique. All polymer-coated NPs at varied doses (1.6, 1.6, and 1.2 µg/ml) showed inhibitory effects. The highest inhibition zone (29 mm) was observed with PEG-coated $Fe_2O_3$ (1.6 µg/ml) and PEG-coated Ag NPs (1.2 µg/ml), while the lowest (25 mm) was with PEG-coated $Al_2O_3$ (1.6 µg/ml). Gram-positive bacteria showed higher sensitivity to these NPs than Gram-negative bacteria, consistent with previous findings [31] (**Figure 33**, **Table 4**) [12].

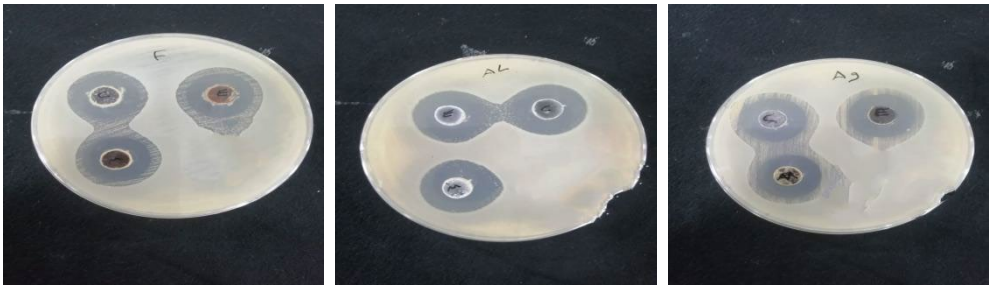

**Figure 33.** Antibacterial activity of biogenic polymer (CMC, MC, PEG) coated NPs against B. subtilis.

**Table 2.** Inhibition zone of B. subtilis by polymer-coated NPs.

| Bacteria | Polymers | $Fe_2O_3$ (1.6 µg/ml) | $Al_2O_3$ (1.6 µg/ml) | Ag (1.2 µg/ml) |
|---|---|---|---|---|
| B. subtilis | CMC | 28 | 26 | 29 |
| | MC | 28 | 28 | 27 |
| | PEG | 29 | 25 | 29 |

## 4. Conclusions

In this work, $Fe_2O_3$, $Al_2O_3$, and Ag nanoparticles were coated with carboxymethylcellulose (CMC) polymer using a simple hydrothermal technique. The ability of as-prepared nanosolutions to remove crude oil from water was systematically investigated. Key findings include: (1) CMC-coated Ag nanoparticles demonstrated the highest oil removal efficiency, achieving 100% removal at 1.2 wt% loading within 24 hours; (2) CMC-$Fe_2O_3$ and CMC-$Al_2O_3$ achieved 97-98% removal at 1.6 wt% loading; (3) The order of effectiveness was Ag > $Fe_2O_3$ > $Al_2O_3$, attributed to differences in surface area, particle size, and adsorption capacity; (4) GC-MS analysis confirmed complete removal of C9-C21 alkanes within 6 hours and >67% removal of C22-C25 alkanes within 24 hours. The superior performance of CMC-Ag nanoparticles is attributed to their homogeneous morphology, small particle size, high surface energy, and strong hydrophobic interactions with crude oil components. Antibacterial studies showed that all polymer-coated NPs exhibited inhibitory activity against B. subtilis, with Gram-positive bacteria being more sensitive than Gram-negative bacteria. Practical applications of this research include: (1) Emergency response to marine and freshwater oil spills; (2) Treatment of oily industrial wastewater; (3) Protection of sensitive coastal ecosystems and aquaculture facilities. Future work should focus on field-scale trials, optimization of environmental parameters (pH, temperature, salinity), and comprehensive ecotoxicological assessment to facilitate large-scale implementation.

## Conflict of interest

The authors declare no conflict of interest

## References


1. National Commission on the BP Deepwater Horizon Oil Spill and Offshore Drilling. Deep Water: The Gulf Oil Disaster and the Future of Offshore Drilling. Washington, DC: US Government Printing Office; 2014.
2. US Environmental Protection Agency (EPA). Cruise Ship Discharge Assessment Report. EPA 842-R-07-005; 2008.
3. Yoshioka G, Carpenter M. Characteristics of reported inland and coastal oil spills. US Environmental Protection Agency; 2002.
4. Aldy JE. Real-time economic analysis and policy development during the BP Deepwater Horizon oil spill. Vanderbilt Law Review. 2011;64(6):1795–1817.
5. Fingas M. The Basics of Oil Spill Cleanup. 2nd ed. Boca Raton: Taylor & Francis; 2000.
6. Harvey S, Elashvili I, Valdes JJ, Kamely D, Chakrabarty AM. Enhanced removal of Exxon Valdez spilled oil from Alaskan gravel by a microbial surfactant. Nat Biotechnol. 1990;8(3):228–230.
7. Federal Interagency Solutions Group. Oil Budget Calculator: Deepwater Horizon—Technical Document. NOAA; 2010.
8. NOAA. Environmental impacts of dispersants. Available from: http://response.restoration.noaa.gov
9. Atlas RM, Hazen TC. Oil biodegradation and bioremediation: a tale of the two worst spills in U.S. history. Environ Sci Technol. 2011;45(16):6709–6715.
10. Deng D, Prendergast DP, MacFarlane J, Bagatin R, Stellacci F, Gschwend PM. Hydrophobic meshes for oil spill recovery devices. ACS Appl Mater Interfaces. 2013;5(3):774–781.
11. Lahann J. Environmental nanotechnology: nanomaterials clean up. Nat Nanotechnol. 2008;3(6):320–321.
12. Fabrega J, Luoma SN, Tyler CR, Galloway TS, Lead JR. Silver nanoparticles: behaviour and effects in the aquatic environment. Environ Int. 2011;37(2):517–531.
13. Chen X. Molecular Imaging Probes for Cancer Research. World Scientific; 2012.
14. Gong JL, Wang B, Zeng GM, Yang CP, Niu CG, Niu QY, Zhou WJ, Liang Y. Removal of cationic dyes from aqueous solution using magnetic multi-wall carbon nanotube nanocomposite as adsorbent. J Hazard Mater. 2009;164:1517–1522.
15. Sharma YC, Srivastava V, Singh VK, Kaul SN, Weng CH. Nano-adsorbents for the removal of metallic pollutants from water and wastewater. Environ Technol. 2009;30(6):583–609.
16. Wu L, Zhang J, Li B, Wang A. Magnetically driven super durable superhydrophobic polyester materials for oil/water separation. Polym Chem. 2014;5(7):2382–2390.
17. Calcagnile P, Fragouli D, Bayer IS, Anyfantis GC, Martiradonna L, Cozzoli PD, Cingolani R, Athanassiou A. Magnetically driven floating foams for the removal of oil contaminants from water. ACS Nano. 2012;6(6):5413–5419.
18. Ge B, Zhang Z, Zhu X, Men X, Zhou X. A superhydrophobic/superoleophilic sponge for the selective absorption of oil pollutants from water. Colloids Surf A. 2013;429:129–133.

19. Nguyen DD, Tai NH, Lee SB, Kuo WS. Superhydrophobic and superoleophilic properties of graphene-based sponges fabricated using a facile dip coating method. Energy Environ Sci. 2012;5(7):7908–7912.
20. Mansoori GA, Bastami TR, Ahmadpour A, Eshaghi Z. Environmental application of nanotechnology. Annual Review of Nano Research. 2008;2:439–493.
21. BP. Gulf Science Data Reference: Oil Characterization Data. 2014.
22. Silverstein RM, Webster FX, Kiemle DJ. Spectrometric Identification of Organic Compounds. 7th ed. Wiley; 2005.
23. Pretsch E, Bühlmann P, Badertscher M. Structure Determination of Organic Compounds: Tables of Spectral Data. 4th ed. Springer; 2009.
24. Pavia DL, Lampman GM, Kriz GS, Vyvyan JA. Introduction to Spectroscopy. 4th ed. Brooks/Cole; 2009.
25. Law AT. Acute and chronic toxicity of Malaysian crude oil water-soluble fraction. ASEAN Marine Environmental; 1997.
26. Song JE, Phenrat T, Marinakos S, Xiao Y, Liu J, Wiesner MR, Tilton RD, Lowry GV. Hydrophobic interactions of nanoparticles increase sorption of phenanthrene. Environ Sci Technol. 2011;45(14):5988–5995.
27. Baalousha M, Nur Y, Römer I, Tejamaya M, Lead JR. Effect of monovalent and divalent cations, anions and fulvic acid on aggregation of citrate-coated silver nanoparticles. Sci Total Environ. 2013;454–455:119–131.
28. Coey JMD. Magnetism and Magnetic Materials. Cambridge University Press; 2010.
29. Palchoudhury S, Lead JR. A facile and cost-effective method for separation of oil–water mixtures using polymer-coated iron oxide nanoparticles. Environ Sci Technol. 2014;48(24):14558–14563.
30. Ehsanizadeh SA, Ahmadi-Kashani M, Abdulhusain ZH, Abed MJ, Salavati-Niasari M. Highly efficient ZnCo2O4 nanospheres and ZnCo2O4/GO nanocomposites as visible light photocatalysts for degradation of organic pollutants. Appl Water Sci. 2025;15(6):128.